Response to Review1

In this study, the authors examined relationship between the snow cover over East Europe and West Siberia (SCES) and the number of haze days in December in central North China (DHDCNC). They found changes in SCES can contribute to DHDCNC through influencing soil moisture and land surface radiation during 1998–2016 but the effects are negligible during 1979–1997. This work is interesting and merits publication after following comments addressed.

General Comments:

1. **The authors explained how changes in soil moisture and radiation lead to the atmospheric circulations worsening dispersion conditions. There are a lot of meteorological fields and effects including in the mechanism. It is better to add a diagram illustrating all the effects.**

Reply:

A new diagram was drawn to make the understanding easier. In "Conclusions and Discussions", we mentioned that "To exemplify the associated mechanisms during 1998–2016, a diagram was drawn and supplemented as Figure S3."

Revisions:

In "Conclusions and Discussions"

……To exemplify the associated mechanisms during 1998–2016, a diagram was drawn and supplemented as Figure S3.

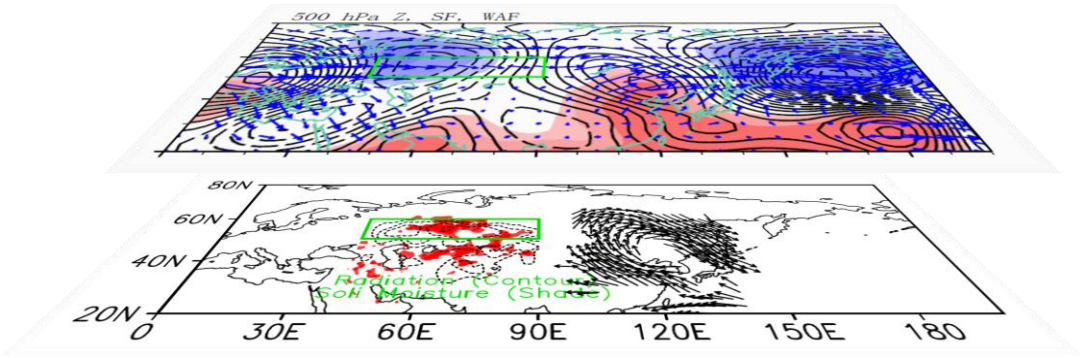

Figure S3. Diagram of the associated physical mechanisms. Near surface, the ON radiation (contour) and soil moisture (shade) were influenced by the SC_{ES}. On the mid-high level, the teleconnected Rossby wave-like pattern propagated into the Central North China, representing by Z500 (shade), stream function (contour) and wave activity flux (arrow). Finally, the local anti-cyclonic circulation near surface

(arrow) led to weak ventilation conditions in December.

2. **The authors examined the relationships of SCES and DHDCNC based on the analysis of correlation coefficient. So one question raises, is it possible that they are independent but covary with each other driven by other factors (e.g., climate change).**

Reply:

The emphasis of this study was the **interannual variation** of haze days and its relationship with snow cover. Thus, during analyzing, the linear trend was removed.

In our study, we assumed that the energy consumption linearly increased in the recent years. On such hypothesis, the human activities (also including **the climate change**) mainly impacted the long-term trend of DHD_{CNC}. **After removal of the linear trend, the interannual variability of haze pollution should be mainly the result of climatic anomalies.**

In the revisions, the authors also **supplemented some previous studies on the long-term trend of haze pollutions**, i.e., the impacts of climate change.

Revisions:

In "Introduction"

……For the long-term trend of haze pollution, Wang and Chen (2016) illustrated the roles of climate change on the in eastern China and emphasized the effects of the Arctic sea ice. Cai et al (2017) analyzed the weather conditions conductive to Beijing severe haze more frequent under climate change. There were also previous studies on the interannual variation of haze and associated climatic conditions. The possible physical processes in the atmosphere that caused this the haze events……

3. **The author mentioned Eurasian snow cover has been increasing over the last two decades (Cohen et al. 2012). What is the mechanism for the increasing SCES.**

Reply:

An associated reference was cited to answer this question. "Different from the

declining trend of Arctic sea ice, Eurasian snow cover has been increasing over the last two decades (Cohen et al. 2012), probably due to **the increased southward moisture transport from the melted Arctic Ocean** (Deser et al., 2010)."

Revisions:

In "Introduction"

Different from the declining trend of Arctic sea ice, Eurasian snow cover has been increasing over the last two decades (Cohen et al. 2012), probably due to the increased southward moisture transport from the melted Arctic Ocean (Deser et al., 2010)……

Deser, C., R. Tomas, M. Alexander, and D. Lawrence. 2010. The seasonal atmospheric response to projected Arctic sea ice loss in the late twentyfirst century, J. Clim., 23(2), 333–351, doi:10.1175/2009JCLI3053.1.

4. **In addition, based on the positive correlation coefficient between SCES and DHDCNC, does that mean the increasing snow cover in Eurasia lead to the increasing aerosol pollution in China during recent decades? If so, it is more interesting and the authors may discuss more about it.**

Reply:

In this manuscript, we used the haze days to **represent the general of haze pollution**. During 1998–2016, the accumulated snow cover significantly intensified the haze pollution in Central North China by atmospheric teleconnection.

Specific comments:

Line 26: typo '/'.

Reply:

The error has been corrected.

Revisions:

In December 2016, central North China (CNC, located at 30–41 ºN, 110–120 ºE),

Line 29: Recent studies found, in additions to emissions and climate change,

aerosolmeteorology feedbacks have contributed the haze in China (e.g., Ding et al., 2016;Yang et al., 2017a).

Reply:

The advice was adopted. Some revisions and new references were added.

Revisions:

In "Introduction"

Beyond anthropogenic emissions, the atmospheric circulations (Yin and Wang 2017b) and **aerosol-meteorology feedback (Ding et al. 2016, Yang et al. 2017a)** have significantly contributed the severe haze in China.

Yang, Y., L. M. Russell, S. Lou, H. Liao, J. Guo, Y. Liu, B. Singh, and S. J. Ghan, Dustwind interactions can intensify aerosol pollution over eastern China, Nat. Commun., 8, 15333, doi:10.1038/ncomms15333, 2017a.

Line 37: Besides to less ventilation, transport of aerosols from upwind can also lead to regional aerosol pollution (e.g., Yang et al., 2017b).

Reply:

The advice was adopted. Some revisions and new references were added.

Revisions:

In "Introduction"

……Furthermore, the southerly anomalies that are characteristic of East Asian winter monsoons (Li et al. 2015; Yin et al. 2015) may have weakened the cold air and wind speed but enhanced **the transportation of humid air flow and aerosols (Yang et al. 2017b)**……

Yang, Y., Wang, H., Smith, S. J., Ma, P.-L., and Rasch, P. J.: Source attribution of black carbon and its direct radiative forcing in China, Atmos. Chem. Phys., 17, 4319-4336, https://doi.org/10.5194/acp-17-4319-2017, 2017b.

Line 124: How can surface upward motion appears in a sinking motion atmosphere. Upward motion sometimes means non-stagnation and strong dispersion. How can it accumulate aerosols?

Reply:

We have corrected the discussions about the vertical motion.

1. There was significant **upward motion near surface (Figure 5a), indicating weak convergences of the aerosols discharged in the circumjacent regions**. Actually, in winter, the weak convergence near surface was a classical synoptic situation resulting in severe haze pollution. This convergence could transport the aerosols discharged in the surrounding to the CNC area, but cannot disturbed the shallow boundary layer. **The converging and local aerosols both accumulated and reached a high concentration**.

2. The description of the sinking motion on the **mid-high level** was not precise and has been **deleted** from this manuscript on the premise that the conclusions were not affected. In a recent study, we have found that **the vertical motions below different parts of the anti-cyclonic circulation were also different**. It is inaccurate to simply describe the associated vertical velocity as sinking or ascending motion. Thus, we are going to write a new manuscript to discuss the associated vertical motions.

Revisions:

In "Possible physical mechanisms"

……The associated vertical velocity at the surface was upward (Figure 5a), indicating weak convergences of the aerosols discharged in the circumjacent regions. However, due to the shallower planetary boundary layer (Figure 5a), the converging and local aerosols cannot be dispersed into the upper atmosphere. The local convergences, combined with the weak surface wind (Figure 5b), easily enabled aerosols to accumulate over the CNC area……

~~The sinking motion caused by these anti-cyclonic anomalies could~~ _ ~~lead to the shallower planetary boundary layer (Figure 5a) and the rather weak dispersion capacity of atmospheric particulates. In contrast, t~~The associated vertical velocity at the surface was upward (Figure 5a), indicating ~~an ascending motion~~ _ convergences of the aerosols discharge in the circumjacent regions. However, ~~near the surface.~~ due to the shallower planetary boundary layer (Figure 5a), the converging and local aerosols cannot be dispersed into the upper atmosphere. The local ~~rising air~~convergences, combined with the weak ~~south~~ surface wind (Figure 5b), easily enabled aerosols to accumulate over the CNC area. Near the surface, the positive SLP anomalies were situated in the east of China and the western Pacific (Figure 5c). The stimulated southerlies overlapped with

Line 166: Why the "west wet-east dry" pattern leads to poor dispersion conditions?

Reply:

This is still an open question and beyond the scope of this study. In the final section, we discussed that this question should be **a future work** with numerical models.

Revisions:

In "Conclusions and Discussions"

……In this study, the varied relationship between the SC_{ES} and DHD_{CNC} and the associated physical mechanisms were analyzed, but more detailed investigations, **such as the internal processes driving how the soil moisture (radiative cooling) impacted the atmosphere in the following December, were not included in this study and should be conducted with numerical models in future work**……

Line 172: What is the direction for positive longwave and shortwave radiation defined in this study? Also, the authors should make clear that they are the surface net radiative fluxes.

Reply:

The upward radiation is positive. The description on the radiation dataset was improved to make it clearer.

Revisions:

In "Datasets and methods"

……the vertical wind, the **surface** net longwave radiation and the **surface** net shortwave radiation **(upward radiation is positive)** data were downloaded from……

Response to Review2

This study discussed the effect of Eurasian snow cover on December haze days. Recently, severe haze occurs in the broad area of China, and the discussion of the relationship between Eurasian snow cover on December haze days is helpful to understand the mechanism modulation the formation of haze. The topic is interesting and I have a few questions listed below:

1. **Line 124: The authors said "In contrast, the associated vertical velocity at the surface was upward, indicating an ascending motion near the surface." I think the downward vertical velocity favors the haze formation due to weak dispersion conditions. The authors published a paper in 2017 (Atmos. Chem. Phys.,17, 11673–11681, 2017 https://doi.org/10.5194/acp-17-11673-2017), and in Figure 7, the omega was positive, and the authors stated that "Under their influence, there was a descending motion from 30 to 55_ N (Fig. 7)," and claimed this condition support the severe haze. Thus, the statement regarding the vertical motion in this study is somewhat contradicts with the previous study.**

Reply:

We have corrected the discussions about the vertical motion.

1. There was significant **upward motion near surface (Figure 5a), indicating weak convergences of the aerosols discharged in the circumjacent regions**. Actually, in winter, the weak convergence near surface was a classical synoptic situation resulting in severe haze pollution. This convergence could transport the aerosols discharged in the surrounding to the CNC area, but cannot disturbed the shallow boundary layer. **The converging and local aerosols both accumulated and reached a high concentration**.

2. The description of the sinking motion on the **mid-high level** was not precise and has been **deleted** from this manuscript on the premise that the conclusions were not affected. In a recent study, we have found that **the vertical motions below different parts of the anti-cyclonic circulation were also different**. It is inaccurate to simply describe the associated vertical velocity as sinking or ascending motion. Thus, we are

going to write a new manuscript to discuss the associated vertical motions.

Revisions:

In “Possible physical mechanisms”

……The associated vertical velocity at the surface was upward (Figure 5a), indicating weak convergences of the aerosols discharged in the circumjacent regions. However, due to the shallower planetary boundary layer (Figure 5a), the converging and local aerosols cannot be dispersed into the upper atmosphere. The local convergences, combined with the weak surface wind (Figure 5b), easily enabled aerosols to accumulate over the CNC area……

~~The sinking motion caused by these anti-cyclonic anomalies could~~ ~~lead to the shallower planetary boundary layer (Figure 5a) and the rather weak dispersion capacity of atmospheric particulates. In contrast, t~~The associated vertical velocity at the surface was upward (Figure 5a), indicating ~~an ascending motion~~ convergences of the aerosols discharge in the circumjacent regions. However, ~~near the surface.~~ due to the shallower planetary boundary layer (Figure 5a), the converging and local aerosols cannot be dispersed into the upper atmosphere. The local ~~rising air~~convergences, combined with the weak ~~south~~ surface wind (Figure 5b), easily enabled aerosols to accumulate over the CNC area. Near the surface, the positive SLP anomalies were situated in the east of China and the western Pacific (Figure 5c). The stimulated southerlies overlapped with

2. **References: It is easier to read if a few spaces were left in front of the first line of each reference. Alternatively, a number can be used to separate each reference as well.**

Reply:

The advice was adopted.

Revisions:

under Climate Change. Nature Climate Change. doi:10.1038/nclimate3249

Chen H. P., Wang H. J. 2015. Haze days in North China and the associated atmospheric circulations based on daily visibility data from 1960 to 2012. J. Geophys. Res. Atmos. 120(12): 5895–5909 DOI: 10.1002/2015JD023225.

Cohen J L, Furtado J C, Barlow M A, Alexeev V A, Cherry JE. 2012. Arctic warming, increasing snow cover and widespread boreal winter cooling. Environ Res Lett 7:014007

Cohen J, Barlow M, Kushner PJ, Saito K. 2007. Stratosphere and troposphere coupling and links with Eurasian land surface variability. J Climate. 20:5335–5343

Dee D. P., Uppala S. M., Simmons A. J., Berrisford P., Poli P., Kobayashi S., Andrae U., Balmaseda M. A., Balsamo G.,

3. Line 59: "Basing on" should be "based on"

Reply:

The error has been corrected.

Revisions:

……Zou et al (2017) also pointed out that there was close relationship between Eurasia snow and haze in China **based on** the observational and numerical analysis……

4. Line 100-103: The authors declared that "during P2, the snow cover with larger interannual variation was distributed widely and zonally": do you have a figure displaying the distributions of the snow cover? It is hard to tell without a figure how the snow cover was spatially distributed.

Reply:

Due to our poor expression, there was some confusion. What we wanted to show was **the intensity of interannual variations**. In the revision, we clarified the intensity of the interannual variations was described by the **standard deviation in Figure 2 (green lines)**.

Revisions:

In "Strengthening relationship and associated atmospheric circulations"

……However, during P1, the CC over the east part of the ES area was insignificant. **The intensity of the interannual variations (i.e., expressed by the standard deviation in Figure 2)** in snow cover over the Tibet Plateau and Mongolian Plateau were evident both during P1 and P2……

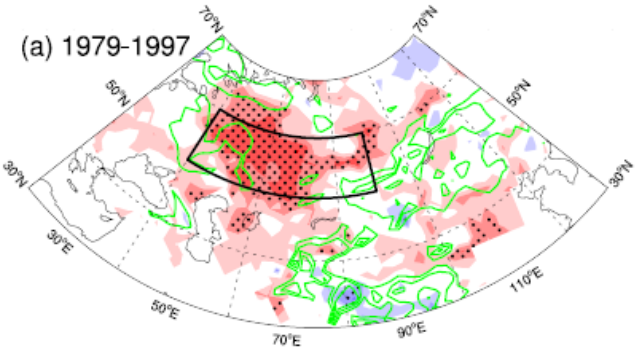

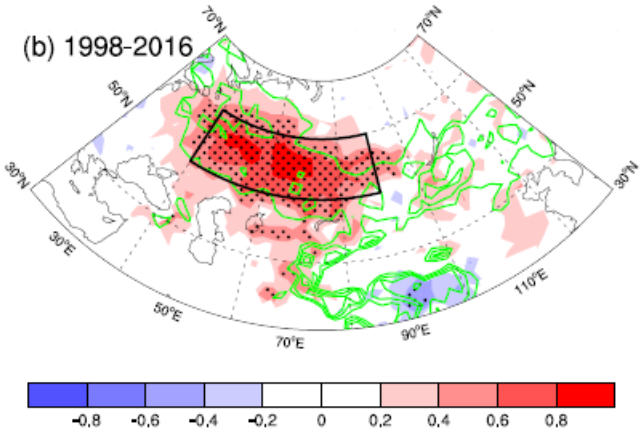

Figure 2 The CC between the SC_{ES} and snow cover (a) from 1979 to 1997 and (b) from 1998 to 2016. The black dots indicate the CC exceeded the 95% confidence level (t test). The black box represents the ES area. The linear trend is removed. **The green lines indicate that the interannual variations in snow cover were obvious in this region.**

5. **There are a few places which did not clearly mention the figure number, which makes it hard to follow. For example: Line 145: In the first paragraph of the section 4 "possible physical mechanisms", the authors should mention Figure 9 first, so the readers can follow the authors easily. Otherwise, it is hard to know which figure the authors are referring to. Line 176: RL1. . ., this information is from Figure 11a, so the authors should point out Fig. 11a immediately after the description.**

Reply:

The error has been corrected. Furthermore, the similar errors were checked and revised throughout the manuscript.

Revisions:

In "Possible physical mechanisms"

……The associated anomalous circulations tended to lead local meteorological conditions (e.g., higher BLH and more obvious surface wind speed) to favor ventilation **(Figure 8)**, which was consistent with the 21-yr running CC in Figure 1a (i.e., negative before the mid-1990s)……

……During P2, the SCES was significantly positively correlated with soil moisture around the Caspian Sea, Balkhash Lake, and Ural Mountains (**Figure 9**, RM1: 50–80oE, 40–60 ℃N)……

……this was denoted as RS1 (70–100 ℃, 38–58 ℃) and was mountainous (**Figure 11c**). In contrast, the regions that had significant and negative CCs and net longwave radiation were smaller and over the Pamir Mountains (**Figure 11a**, RL1: 67.5–90 ℃, 36–45 ℃). By contrast, the significant correlated regions with net longwave radiation (**Figure 11b**, RL2) and net shortwave radiation **(Figure 11d**, RS2) were the same and nearly overlapped with the ES area during P2, which was wider and had a zonal distribution……

6. **Line 180: if there was more SCES, the absolute value of the net longwave radiation and net shortwave radiation would both be smaller. The signs of the correlations between SCES and net longwave radiation, SCES and net shortwave radiation are opposite. I am not sure why the absolute value of the net longwave radiation and net shortwave radiation would both be smaller when there was more SCES**

Reply:

The upward radiation is positive. Shown by the Figure below, the net surface short wave radiation was globally negative. However, the net surface long wave radiation was globally positive. Thus, the more significant positive correlation with short wave radiation and negative correlation with long wave radiation both meant the radiation reduced, i.e., the net shortwave and net longwave radiations were both reduced.

To make the analysis clearer, the writing was improved both in the section "dataset" and in the section "physical mechanism".

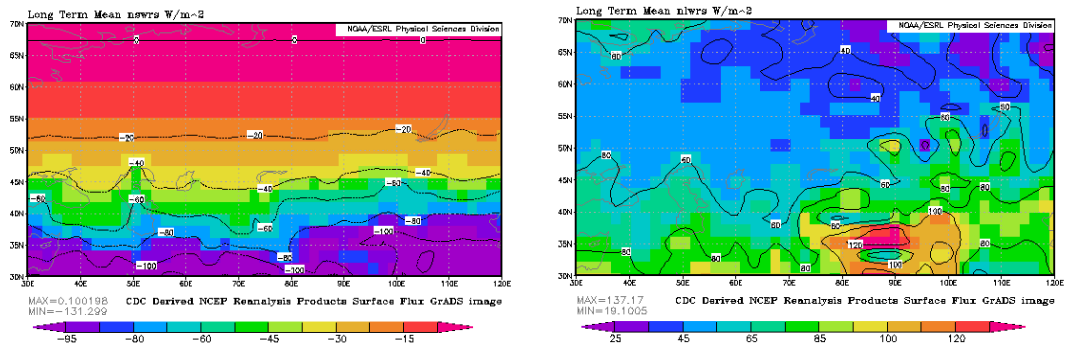

Figure the net surface short wave radiation (left) and net surface long wave radiation (right) in December, directly plotted by the website of NOAA/NCEP PSD

Revisions:

In “Datasets and methods”

……the vertical wind, the **surface** net longwave radiation and the **surface** net shortwave radiation **(upward radiation is positive)** data were downloaded from……

In “Possible physical mechanisms”

……As a feedback, the outgoing longwave radiations emitted by the cooler land surface were weakened and had radiative cooling impacts on the atmosphere (Zhang et al. 2017). **That is to say: the absorbed shortwave and outgoing longwave radiations were both reduced**……

……According to the above analysis, if there was more SC_{ES}, the net shortwave and net longwave radiations were both reduced, i.e., the absolute value of the net longwave radiation and net shortwave radiation would both be smaller……

7. Line 197: EAJS was shifted significantly northward Without a base location, how can this shift be identified?

Reply:

The climatic distribution of U200 was showed below. The location of EAJS was around 30°N. In Figure 3, the U200 anomalies were negative near 30°N, but positive northward. Thus, EAJS was shifted significantly northward. If, we plotted the climatic distribution of U200 in the Figures of the manuscript, the Figures should become too complicated and take up too much space. After careful thought, the climatic distribution of U200 was still omitted.

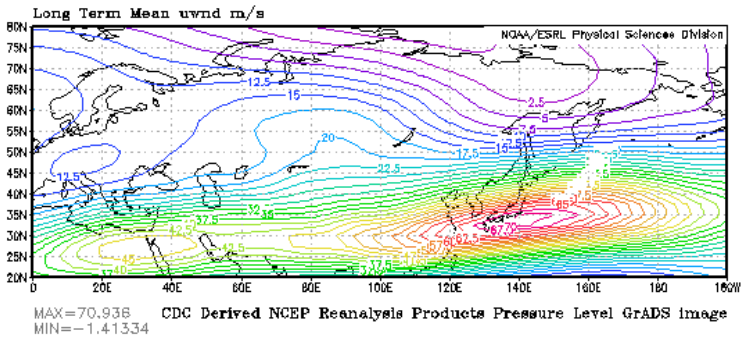

Figure the climatic distribution of U200, directly plotted by the website of NOAA/NCEP PSD

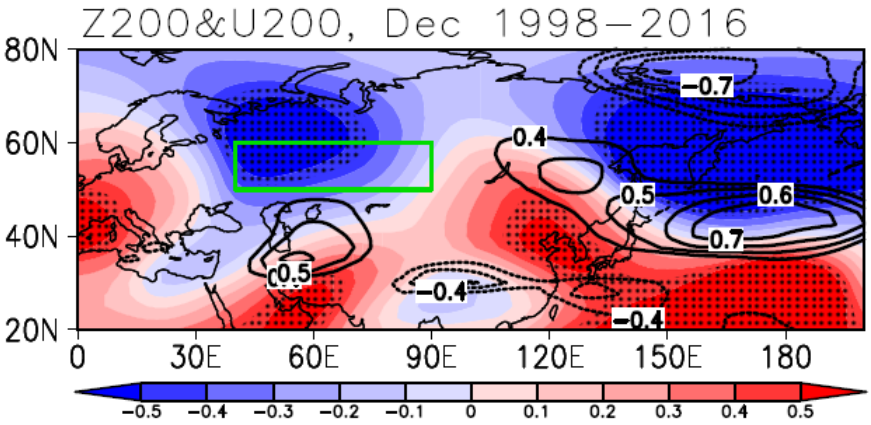

Figure 3 The CC between the SCES and Z200 (shading) and U200 (contour) in December from 1998 to 2016. The black dots indicate the CC exceeded the 95% confidence level (t test). The green box represents the ES area. The linear trend is removed.

8. The figure qualities and descriptions of captions need to be improved: For example: Figure 1: CCdt, CCOS should be explained in the caption. A figure is in principle can be independent from the paper. Thus, one should get all the information from the figure or caption without searching from the main text.

Reply:

The error has been corrected. Furthermore, the similar errors were checked and revised throughout the manuscript.

Revisions:

Figure 1 (a) the variation of the normalized DHD_{CNC} (black) and SC_{ES} (blue) from 1979 to 2016 after detrending and the 21-yr running correlation coefficient (CC) between the DHD_{NH} and SC_{ES} before (solid, red) and after (dash, red) detrending. (b) The CC between the DHD_{CNC} and snow cover from 1979 to 2016 after detrending. The black dots indicate CCs exceeding the 95% confidence level (t test). The black box represents the ES area. **The subscript "dt" and "OS" in panel (a) represented the CC was calculated by the detrending and original sequence.**

Figure 9 The CC between the SC_{ES} and soil moisture in (a) October-November and (c) December from 1979 to 1997, and in (b) October-November and (d) December from 1998 to 2016. The black dots indicate the CC exceeded the 95% confidence level (t test). The linear trend is removed. The green boxes **(RM1 and RM2)** are the significantly correlated areas, which were used to calculate the SoilM index.

Figure 11 The CC between the SC_{ES} and (a) longwave radiation and (c) shortwave radiation in October-November from 1979 to 1997 and the CC between the SC_{ES} and (b) longwave radiation and (c) shortwave radiation in October-November from 1998 to 2016. The black dots indicate the CC exceeded the 95% confidence level (t test). The linear trend is removed. The green boxes **(RL and RS)** are the significantly correlated areas, which were used to calculate the I_{LS1} (I_{LS2}).

The Strengthening Relationship between Eurasian Snow Cover and December Haze Days in Central North China after the Mid-1990s

Zhicong Yin [12] and Huijun Wang [12]

[1]Key Laboratory of Meteorological Disaster, Ministry of Education / Joint International Research Laboratory of Climate and Environment Change (ILCEC) / Collaborative Innovation Center on Forecast and Evaluation of Meteorological Disasters (CIC-FEMD), Nanjing University of Information Science & Technology, Nanjing 210044, China

[2]Nansen-Zhu International Research Centre, Institute of Atmospheric Physics, Chinese Academy of Sciences, Beijing, China

Correspondence to: Zhicong Yin (yinzhc@163.com)

Abstract. The haze pollution in December has become increasingly serious over recent decades and imposes damage on society, ecosystems, and human health. In addition to anthropogenic emissions, climate change and variability were conducive to haze in China. In this study, the relationship between the snow cover over East Europe and West Siberia (SC_{ES}) and the number of haze days in December in central North China was analyzed. This relationship significantly strengthened after the mid-1990s, which is attributed to the effective connections between the SC_{ES} and the Eurasian atmospheric circulations. During 1998–2016, the SC_{ES} significantly influenced the soil moisture and land surface radiation, and then, the combined underlying drivers of enhanced soil moisture and radiative cooling moved the East Asia jet stream northward and induced anomalous, anti-cyclonic circulation over central North China. Modulated by such atmospheric circulations, the local lower boundary layer, the decreased surface wind and the more humid air were conducive to the worsening dispersion conditions and frequent haze occurrences. In contrast, from 1979 to 1997, the linkage between the SC_{ES} and soil moisture was negligible. Furthermore, the correlated radiative cooling was distributed narrowly and far from the key area of snow cover. The associated atmospheric circulations with the SC_{ES} were not significantly linked with the ventilation conditions over central North China. Consequently, the relationship between the SC_{ES} and the number of hazy days in central North China was insignificant before the mid-1990s but has strengthened and has become significant since then.

Keywords. Haze, Aerosol, Snow cover, North China, Climate Variability

1. Introduction

In December 2016, central North China (CNC, located at 30–41°~~/~~N, 110–120°E), where more than 300 million people live, experienced severe haze pollution (Yuan and Ma 2017). On 70% of the days in December 2016, the people who lived in CNC breathed polluted air, which influenced the health of everyone, especially children. Beyond anthropogenic emissions, the ~~influences of~~ atmospheric circulations (Yin and Wang 2017b) and aerosol-meteorology feedback (Ding et al. 2016, Yang et al. 2017a) ~~on~~ have significantly contributed the~~is~~ severe haze in China. ~~event were significant (Yin and Wang 2017b).~~ Many recent previous studies have documented that climate change and variability contributed to the severe winter haze pollution in China (Cai et al. 2017; Ding et al. 2014; Wang and Chen, 2016; Yang et al. 2016). For the long-term trend of haze pollution, Wang and Chen (2016) illustrated the roles of climate change on the in eastern China and emphasized the effects of the Arctic sea ice. Cai et al (2017) analyzed the weather conditions conductive to Beijing severe haze more frequent under climate change. There were also previous studies on the interannual variation of haze and associated climatic conditions. The possible physical processes in the atmosphere that caused ~~this~~ the haze events may have included, when the positive pattern of East Atlantic/West Russia and West Pacific (Yin et al. 2017a) occurred together or partly, the anomalous anti-cyclone over CNC and Japan Sea would be enhanced and then confined the vertical motion of atmospheric matters. Furthermore, the southerly anomalies that are characteristic of East Asian winter monsoons (Li et al. 2015; Yin et al. 2015) may have weakened the cold air and wind speed but enhanced the transportation of humid air flow and aerosols (Yang et al. 2017b). Thus, the vertical and horizontal dispersion capacities were both restricted, which resulted in haze pollution. ~~In regard to~~Concerning external mechanisms, the investigated climatic factors include sea surface temperature (SST) over ~~the North Atlantic (Xiao et al. 2015) and~~ subtropical Western Pacific (Yin and Wang 2016, Gao and Chen 2017), Arctic sea ice (Wang and Chen 2015, 2016) and the topography of the Tibetan Plateau (Xu et al. 2016). In addition, the large-scale SST patterns, such as the El Nino-Southern Oscillation and the Pacific decadal oscillation, also showed close relationships with the haze pollution in the east of China (Gao et al. 2015).

Different from the declining trend of Arctic sea ice, Eurasian snow cover has been increasing over the last two decades (Cohen et al. 2012), probably due to the increased southward moisture transport from the melted Arctic Ocean (Deser et al., 2010). The anomalous snow cover influenced the exchange of heat and moisture in atmosphere-land interactions, which were characterized by high albedo and water effects (Chen et al 2012). Starting in autumn, the snow cover over Eurasia began to accumulate gradually and was significantly correlated with the winter climate in the Northern Hemisphere (Foster

et al. 1983; Zhang et al. 2007; Li and Wang 2014; Li et al 2017; Xu et al. 2017). In October, enhanced snow cover was associated with a negative Arctic Oscillation phase (Gong et al. 2007) via the stratosphere–troposphere coupled planetary wave activity (Cohen et al. 2007). The change in the October-November (ON) Eurasian snow cover was also considered as a primary factor for the recent recovery of the Siberian High intensity over the last few decades (Jeong et al. 2011). Furthermore, there was a significant negative correlation between the October snow cover located in eastern Siberia and in the area northeast of Lake Baikal and the following-winter air temperature over Northeast China (Li et al. 2017). A notable feature related with the impact of snow cover was the change in the relationship with the winter climate in the Northern Hemisphere after the mid-1990s. Both observational evidence and model simulations demonstrated a significant change in the relationship between the autumn Eurasian snow depth and the East Asian winter monsoon (Li and Wang 2014). Xu et al (2017) applied a 15-year sliding correlation to show the intensification in the connection between the October snow cover and the January "warm Arctic-cold Eurasia" pattern since the mid-1990s. Specifically investigating the impact of snow cover on December haze days over the CNC area (DHD_{CNC}), Yin and Wang (2017b) illustrated that DHD_{CNC} significantly related with the ON snow cover over East Europe and West Siberia (SC_{ES}). Zou et al (2017) also pointed out that there was close relationship between Eurasia snow and haze in China ~~basing~~ based on the observational and numerical analysis. Thus, a question raised here was whether there was a significant change in the connection between SC_{ES} and DHD_{CNC}. Motivated by many previous studies, we attempted to answer this question and explored the associated physical mechanisms. The investigation described in this paper will highlight the impact of SC_{ES}, recognize the changes in their relationships with other variables, and improve the seasonal prediction potential of the DHD_{CNC}.

The remainder of this paper is organized as follows. The data and methods are described in section 2. In section 3, we analyzed the strengthening relationship between SC_{ES} and DHD_{CNC}, as well as the associated atmospheric circulations. Then, the possible physical mechanisms were studied in section 4. The main conclusions of this study and necessary discussion material are included in section 5.

2. Datasets and methods

The geopotential height at 500 hPa (Z500) and 200 hPa (Z200), the zonal wind at 200 hPa (U200), the wind at 850 hPa (UV850), the wind speed at the surface, the sea level pressure (SLP), the surface air temperature (SAT), the surface relative humidity, the vertical wind, the surface net longwave radiation and the surface net shortwave radiation (upward radiation is

positive) data were downloaded from the National Center for Environmental Prediction and the National Center for Atmospheric Research. These 2.5°×2.5° reanalysis datasets were available for the period between 1948 and 2016 (Kalnay et al. 1996). In addition, the 1°×1° planetary boundary layer height (BLH) was derived from the ERA-Interim dataset (Dee et al. 2011). The monthly snow cover data were supported by the Rutgers University (Robinson et al. 1993). The sub-daily (i.e., four times per day) routine meteorological observations (i.e., relative humidity, visibility, wind speed, and weather phenomena) were collected by the National Meteorological Information Center, China Meteorological Administration. According to Yin et al. (2017a), the haze data were calculated mainly based on the observed visibility and the relative humidity. Because the interval of the haze data was six hours, we defined a haze day as a day with haze occurring at any of the four times. DHD_{CNC} was the mean number of haze days over the CNC area.

3. Strengthening relationship and associated atmospheric circulations

From 1979 to 1997, interannual variation was the main change mode of the DHD_{CNC}, and the linear sloped trend was not significant (Figure omitted). Thereafter, the decadal component of the DHD_{CNC} became significant; that is, the haze days decreased from 1998 to 2010 but increased rapidly (Figure 1a), reaching more than 21 days in 2016. The minimum number of DHD_{CNC} was 10 days and occurred in 2010, while the maximum, 21 days, appeared in 2016 (Yin and Wang 2017b). As illustrated by Yin and Wang (2017b), the DHD_{CNC} has a significantly close relationship with SC_{ES} between 1979 and 2016 (Figure 1b); SC_{ES} was defined as the area-averaged ON snow cover over East Europe and West Siberia (ES: 40–90°E, 50–60°N). This domain was consistent with the centers of the dominant varied mode calculated by Sun (2017). The positive correlation meant that if there was more SC_{ES}, then the haze pollution would be more severe over the CNC area. From the perspective of temporal variation, the SC_{ES} was more consistent with the DHD_{CNC} after the mid-1990s. Similar to the DHD_{CNC}, the maximum and minimum values of the SC_{ES} were also observed in 2016 and 2010, respectively. It appeared that the correlation before the mid-1990s was not significant. Chronologically, the SC_{ES} decreased from 2000 to 2010, but it increased thereafter, which was similar to the DHD_{CNC}. Thus, the 21-yr running correlation coefficient (CC) between the DHD_{CNC} and SC_{ES} was calculated and plotted in Figure 1a. Obviously, the CC was strengthened and became significant after the mid-1990s, exceeding the 99% confidence level. The CC between the DHD_{CNC} and SC_{ES} during the period ~~between~~ of 1998–2016 (P2) was 0.62 after detrending, which was more significant than that during the period ~~between~~ of 1979–1997 (P1), i.e., only 0.07. The ON Eurasian snow cover correlated with the SC_{ES} was greater, and the CC was also larger during

P2 (Figure 2), indicating that the snow cover covaried more within the key areas and could influence the local and teleconnected climate more significantly. However, during P1, the CC over the east part of the ES area was insignificant. The intensity of the interannual variations (i.e., expressed by the standard deviation in Figure 2) in snow cover over the Tibet Plateau and Mongolian Plateau were evident both during P1 and P2. ~~In contrast, t~~The interannual variation in snow cover over East Europe and West Siberia was larger during P2 than during P1, which was also revealed by empirical orthogonal function analysis (Figure omitted). Furthermore, during P2, the snow cover with larger interannual variation was distributed widely and zonally; in contrast, during P1, the significantly varied snow cover was meridionally instead of zonally and was only located to the north of the Black Sea; thus, it could not have been teleconnected with the haze pollution in China. We speculated that the varied interannual variation of the SC_{ES}~~, which was also revealed by empirical orthogonal function analysis (Figure omitted),~~ possibly influenced the strengthening relationship shown in Figure 1a. The impact of Arctic amplification on East Asian winter climate was significant (Wang and Liu 2016; Zhou 2017). Wang et al (2015) illustrated the decline in Arctic sea ice intensified the haze pollution in eastern China. Thus, we calculated the CC between the SC_{ES} (DHD_{CNC}) and the Arctic sea ice during P1 and P2, respectively. The SC_{ES} was insignificantly correlated with the September–November sea ice during P1 (Figure S1) but was significantly correlated with the ON sea ice over the Barents Sea (above 95% confidence level) during P2 (Figure S2). However, during P2, the CC between the ON sea ice over the Barents Sea and the DHD_{CNC} was not significant, indicating that the Eurasian snow cover was relatively independent of the Arctic sea ice in terms of its impact on haze pollution over the CNC area.

To explore the reasons for the observed strengthening relationship, the associated atmospheric circulations with the SC_{ES} during P2 are shown in Figures 3-5. In the upper troposphere, the induced centers of atmospheric activities appeared as a "+–+–" pattern, including the positive centers located in West Europe, North China and the Japan Sea and the negative centers over the north of the Caspian Sea and Aleutian Islands (Figure 3). This Rossby wave-like pattern also existed and propagated with observed wave activity flux in the mid-troposphere (Figure 4). The positive anomalies over North China and the Japan Sea were connected with the subtropical high in the Pacific, resulting in a strong pressure gradient in the south of the Aleutian low. The East Asia jet stream (EAJS), particularly its western end, was located more northward, meaning that the activities of the Rossby waves were also located more northward, and the cold air moving southward to the CNC area was weak (Chen and Wang 2015). ~~The anomalous anti-cyclone over the CNC area could be observed in the upper (Figure 3), middle (Figure 4) and lower troposphere (Figure 5b). The sinking motion caused by these anti-cyclonic anomalies could~~

~~lead to the shallower planetary boundary layer (Figure 5a) and the rather weak dispersion capacity of atmospheric particulates. In contrast, t~~The associated vertical velocity at the surface was upward (Figure 5a), indicating ~~an ascending motion~~ weak convergences of the aerosols discharged in the circumjacent regions. However, ~~near the surface.~~ due to the shallower planetary boundary layer (Figure 5a), the converging and local aerosols cannot be dispersed into the upper atmosphere. The local ~~rising air~~convergences, combined with the weak ~~south~~ surface wind (Figure 5b), easily enabled aerosols to accumulate over the CNC area. Near the surface, the positive SLP anomalies were situated in the east of China and the western Pacific (Figure 5c). The stimulated southerlies overlapped with the mean flow of the East Asian winter monsoon to weaken the cold northerly winds. The SAT of Eurasia was warmer, and the surface wind speeds over the CNC area were significantly reduced; thus, the horizontal ventilation capacity of the atmosphere over the CNC area was weak, and it was difficult for the air pollutants to disperse. Moreover, the enhanced water vapor transportation by the anomalous southerlies (Figure 5b) provided a beneficial environment for hygroscopic growth, which is an important process for the formation of severe haze pollution. In summary, during P2, the atmospheric circulations and local meteorological conditions, which were related with the SC_{ES}, effectively confined the vertical and horizontal dispersion of atmospheric particles.

For comparison, the associated atmospheric circulations during P1 are shown in Figures 6–8. In the mid and high troposphere, the zonal Rossby wave-like pattern, which existed during P2, could not be identified; rather, another pattern propagated meridionally from the Mediterranean Sea to the polar region and then through Northeast China and the Okhotsk Sea to the West Pacific (Figure 6–7). The wide and zonal cyclonic anomalies located over Northeast China and the Okhotsk Sea strengthened the EAJS and the meridional movement of cold air and resulted in the lower SAT in the east of China. The associated anomalous circulations tended to lead local meteorological conditions (e.g., higher BLH and more obvious surface wind speed) to favor ventilation (Figure 8), which was consistent with the 21-yr running CC in Figure 1a (i.e., negative before the mid-1990s). However, this negative relationship was not significant because the correlated area of BLH and surface wind was too narrow; additionally, the surface vertical motion and relative humidity were not significantly correlated with the SC_{ES} during P1.

4. Possible physical mechanisms

In autumn, the snowfall began in the mid-high latitudes. Because the SAT was not persistently below freezing point, part of the snow melted, and the soil moisture increased. In addition to the snow melt, the accumulated snow cover also reduced the

moisture that evaporated from the land surface. During P2, the SC_{ES} was significantly positively correlated with soil moisture around the Caspian Sea, Balkhash Lake, and Ural Mountains (Figure 9, RM1: 50–80°E, 40–60°N). In addition, when the SC_{ES} was greater, the soil was drier to the northeast of Lake Baikal (RM2: 100–130°E, 52.5–62.5°N). These two significant correlations persisted and were enhanced in December, i.e., the CC between the ON snow cover and the December soil moisture was larger than that between the ON snow cover and the ON soil moisture, both in the RM1 and RM2 areas. The area-averaged soil moisture in RM1 (RM2) was denoted as $SoilM_{RM1}$ ($SoilM_{RM2}$), and the SoilM index was defined as the difference between $SoilM_{RM1}$ and $SoilM_{RM2}$ (i.e., $SoilM = SoilM_{RM1} – SoilM_{RM2}$). During P2, the CC between the DHD_{CNC} and the ON (December) SoilM index was 0.69 (0.69) after the removal of the linear trend, and it exceeded the 99% confidence level; however, these significant correlations did not exist during P1 (Table 1). We speculated that the ON snow cover could impact the soil moisture in the RM1 and RM2 areas, which could last into December, and then influence the December haze pollution through atmospheric circulations. Thus, the associated atmospheric circulations in the mid-troposphere were calculated and shown in Figure 10. During P1, the impacts of the SoilM index on Z500 were not significant in ON or December, but this was consistent with the weak relationships between the SC_{ES} and DHD_{CNC}. In contrast, the significantly induced atmospheric circulations were distributed as a zonal Rossby wave-pattern during P2 (Figure 10 b, d), which is similar to the data shown in Figure 4. Particularly, the anomalous anti-cyclonic circulation over the CNC area was significant both in ON and December and was connected with the weak dispersion capacities of the atmospheric particles. The possible physical processes causing this could include the larger snow cover increasing the local soil moisture by melting and impeding evaporation, and the wetter land surface may have persisted and been enhanced in December. The “west wet-east dry” pattern of soil moisture could influence the atmospheric circulations, which would benefit the occurrence of haze pollution as a result of poor dispersion conditions. During P1, both the CC between the SC_{ES} and the SoilM index and the CC between the SoilM index and the DHD_{CNC} were not significant, indicating that the snow cover in the study area did not impact the DHD_{CNC} through effects on land surface moisture.

High albedo is another obvious characteristic of snow cover, which reflects more solar shortwave radiation and results in lower SAT. As a feedback, the outgoing longwave radiations emitted by the cooler land surface were weakened and had radiative cooling impacts on the atmosphere (Zhang et al. 2017). That is to say: the absorbed shortwave and outgoing longwave radiations were both reduced. As shown in Figure 11, the correlated areas of radiation, including the location and shape, were apparently different during these two periods. During P1, the significant CCs between the SC_{ES} and net

shortwave radiation were distributed from the southwest (i.e., Pamir Mountains) to the northeast (i.e., Sayan Mountains); this was denoted as RS1 (70–100°E, 38–58°N) and was mountainous (Figure 11~~b~~c). In contrast, the regions that had significant and negative CCs and net longwave radiation were smaller and over the Pamir Mountains (Figure 11a, RL1: 67.5–90°E, 36–45°N). By contrast, the significant correlated regions with net longwave radiation (Figure 11b, RL2) and net shortwave radiation (Figure 11d, RS2) were the same and nearly overlapped with the ES area during P2, which was wider and had a zonal distribution. According to the above analysis, if there was more SC_{ES}, the net shortwave and net longwave radiations were both reduced, i.e., the absolute value of the net longwave radiation and net shortwave radiation would both be smaller. To assess the combined effects of radiation, the I_{LS} index was defined as the sum of the absolute value of the area-averaged net shortwave radiation ($|I_{RS}|$) and the absolute value of the area-averaged net longwave radiation ($|I_{RL}|$), i.e., $I_{LS1} = |I_{RL1}| + |I_{RS1}|$ and $I_{LS2} = |I_{RL2}| + |I_{RS2}|$. It was obvious that when there was more snow cover, the I_{LS1} and I_{LS2} should be smaller. After removing the linear trend, the CCs between I_{LS} and DHD_{CNC} were calculated and were 0.07 (I_{LS1}, not significant) and –0.72 (I_{LS2}, above 99% confidence level). We speculated that the ON snow cover would influence the December haze pollution by modulating the radiation during P2, but this process did not exist during P1. In fact, Cohen et al (2007) noted that the diabatic cooling in late autumn, which was in accordance with the higher-than-normal snow cover, locally induced higher SLP anomalies and colder SAT; then, significant influences on the tropospheric atmosphere were observed the following winter through stratosphere-troposphere coupling. During P2, because of radiative cooling, the ON SAT was lower over the ES area and was zonally spread to the Okhotsk Sea. Positive ON SLP anomalies were also stimulated in the mid-high latitudes of Eurasia. The induced SLP and SAT anomalies were zonal and almost occupied the mid-high latitudes of Eurasia. In contrast, the SLP and SAT anomalies during P1 were more meridional and smaller and were more westward and located over Europe (Figure 12). Consistent with the radiative drivers from the underlying surface (i.e., radiative cooling), during the following December, the atmospheric responses were more zonal during P2 but tended to be meridional during P1. Moreover, the atmospheric responses during P2 were stronger than those during P1 (Figure 13). The induced Rossby wave-pattern and anomalous EAJS during P2 (P1) were similar with those in Figures 3 (6) and 4 (7). Because of the deep anti-cyclonic anomalies over North China and the subtropical West Pacific, the west end of EAJS was shifted significantly northward, resulting in weak cold air activities during the following December. In the mid-troposphere, there were Z500 anomaly centers located over West Europe (+), the area north of the Caspian Sea (–), North China and the Japan Sea (+), and the Aleutian Islands (–). The teleconnected pattern impacted the local meteorological conditions, such as a shallower boundary

layer, small surface wind speed and sufficient water vapor, which confined the ventilation capacities of the air over the CNC area. The resulting pattern that appeared is shown in Figure 7, and the pattern propagated through the Mediterranean Sea (+), Northwest Europe (–), the polar region (+), Northeast China and the Okhotsk Sea (–), and the West Pacific (+) and also existed in Figure 13a. The subtropical high was located over the ocean, and the Aleutian Low extended westward to the CNC area. The EAJS was enhanced by the significant gradients, indicating obvious meridional cold air activity. Furthermore, there were no significant responses over the CNC area; thus, the impact on the local ventilation conditions were not obvious and resulted in a weak relationship with the occurrence of haze.

5. Conclusions and discussions

The haze pollution in December has become increasingly serious in the past decade (Figure 1a), and the DHD_{CNC} reached 21 days in 2016. Considering the evident damage of the increasing haze, it is meaningful to study the climatic factors that are closely related to haze in China. Yin and Wang (2017b) illustrated that the snow cover over East Europe and West Siberia influenced the DHD_{CNC} from 1979 to 2016, but they did not give adequate attention to the physical mechanisms. In this study, we found that the relationship between the SC_{ES} and DHD_{CNC} also varied and was strengthened after the mid-1990s. During 1998–2016, the interannual variation in the SC_{ES} was more significant, and the snow cover with larger interannual variation was distributed zonally and occupied the entirety of East Europe and West Siberia; thus, the forcing effects were more effective than those during 1979–1997. The associated soil moisture (partially indicating the water effect) and radiation (related with high albedo) were significantly different during these two periods. The radiative cooling effects of the SC_{ES} during the later period were significant and overlapped with the whole target area of snow cover, which was more zonal, broader, and stronger than those in the period of 1979–1997. The soil moisture was also significantly correlated with the SC_{ES}, which could last to December between 1998 and 2016. In contrast, there was no close relationship between the Eurasian soil moisture and the SC_{ES} from 1979 to 1997. Thus, during 1998–2016, the combined influences of the enhanced soil moisture and the radiative cooling that resulted from the positive SC_{ES} anomalies could cause EAJS to shift northward and stimulate the anti-cyclonic anomalies over the CNC area. Under such atmospheric circulations, the local boundary layer was shallower, the surface wind speed was smaller, and the surface moisture was greater. As a result, the atmospheric particles accumulated easily, and the haze occurred frequently. During 1979–1997, both the linkage between the SC_{ES} and soil moisture and the impacts of soil moisture on atmospheric circulations were negligible. The radiative cooling was the

way in which the SC_{ES} modulated the atmospheric circulations. Nevertheless, the correlated regions of radiation were smaller and meridional, and the resulting atmospheric circulations were not significantly linked to the ventilation conditions. Consequently, the relationship between the SC_{ES} and DHD_{CNC} was insignificant from 1979 to 1997 but was strengthened and became significant after the mid-1990s. To exemplify the associated mechanisms during 1998–2016, a diagram was drawn and supplemented as Figure S3.

In this study, the varied relationship between the SC_{ES} and DHD_{CNC} and the associated physical mechanisms were analyzed, but more detailed investigations, such as the internal processes driving how the soil moisture (radiative cooling) impacted the atmosphere in the following December, were not included in this study and should be conducted with numerical models in future work. Many climatic factors at mid-high latitudes have been documented as effective external drivers, including Arctic sea ice (Wang et al 2015, 2016), Eurasian SAT (Yin et al 2017a), SST in ~~the Atlantic (Xiao et al 2015) and~~ Pacific (Yin and Wang 2017a) and Eurasian snow cover (Yin and Wang 2017b). Some questions raised here include why so many linkages are found in the mid-high latitudes and how they work together to impact the haze pollution in China. This is still an open question that needs to be answered. Another question that deserves more attention is why the relationship shifted in approximately 1998. One of the reasonable speculations was the impact of the Pacific Decadal Oscillation, whose phase also shifted in approximately 1998. The questions mentioned above will be addressed in our future work. As a result of the recent enhancement, the significant relationship possibly improved the potential to predict haze pollution, which is valuable for scientific decision-making related to controlling haze pollution in China.

Acknowledgements

This research was supported by the National Natural Science Foundation of China (41705058 and 91744311), the KLME Open Foundation (KLME1607), the CAS–PKU Partnership Program, and the Startup Foundation for Introducing Talent of Nanjing University of Information Science and Technology (20172007)

References

Cai W. J., Li K., Liao H., Wang H. J., Wu L. X., 2017. Weather Conditions Conducive to Beijing Severe Haze More Frequent under Climate Change. Nature Climate Change. doi:10.1038/nclimate3249

Chen H. P., Wang H. J. 2015. Haze days in North China and the associated atmospheric circulations based on daily visibility data from 1960 to 2012. J. Geophys. Res. Atmos. 120(12): 5895–5909 DOI: 10.1002/2015JD023225.

Cohen J L, Furtado J C, Barlow M A, Alexeev V A, Cherry JE. 2012. Arctic warming, increasing snow cover and widespread boreal winter cooling. Environ Res Lett 7:014007

Cohen J, Barlow M, Kushner PJ, Saito K. 2007. Stratosphere and troposphere coupling and links with Eurasian land surface variability. J Climate. 20:5335–5343

Dee D. P., Uppala S. M., Simmons A. J., Berrisford P., Poli P., Kobayashi S., Andrae U., Balmaseda M. A., Balsamo G., Bauer P., Bechtold P., Beljaars A. C. M. 2011. The ERA-Interim reanalysis: configuration and performance of the data assimilation system. Q. J. Roy. Meteor. Soc., 137: 553–597,doi:10.1002/qj.828

Deser, C., R. Tomas, M. Alexander, and D. Lawrence. 2010. The seasonal atmospheric response to projected Arctic sea ice loss in the late twentyfirst century, J. Clim., 23(2), 333–351, doi:10.1175/2009JCLI3053.1.

Ding Y. H., Liu Y. J. 2014. Analysis of long-term variations of fog and haze in China in recent 50 years and their relations with atmospheric humidity. Sci. China Ser. D: Earth Sci. 57: 36–46 (in Chinese)

Ding A J, Huang X, Nie W, Sun J N, Kerminen V M, Petäjä T, Su H, Cheng Y F, Yang X Q, Wang M H, et al. 2016. Enhanced haze pollution by black carbon in megacities in China. Geophys. Res. Lett., 43, 2873–2879, doi: 10.1002/2016GL067745.

Foster J, Owe M, Rango A. 1983. Snow cover and temperature relationships in North America and Eurasia. J Appl Meteorol. 22: 460–469

Gao H, Li X. 2015. Influences of El Nino Southern Oscillation events on haze frequency in eastern China during boreal winters. International Journal of Climatology. 35(9), 10.1002/joc.4133

Gong G, Cohen J, Entekhabi D, Ge Y. 2007. Hemispheric-scale climate response to Northern Eurasia land surface

characteristics and snow anomalies. Global Planet Change. 56:359–370

Gao Y., Chen D. 2017. A dark October in Beijing 2016. Atmos. Oceanic Sci. Lett., 10 (3): 206–213

Jeong J H, Ou T, Linderholm H W, Kim B M, Kim S J, Kug J S, Chen D L. 2011. Recent recovery of the siberian high intensity. Journal of Geophysical Research Atmospheres, 116(D23), D23102.

Kalnay E., Kanamitsu M., Kistler R., Collins W., Deaven D., Gandin L., Iredell M., Saha S., White G., Woollen J., Zhu Y., Leetmaa A., Reynolds R., Chelliah M., Ebisuzaki W., Higgins W., Janowiak J., Mo K. C., Ropelewski C., Wang J., Jenne R., Joseph D. 1996. The NCEP/NCAR 40-year reanalysis project. Bull. Am. Meteorol. Soc., 77: 437–471, doi: 10.1175/1520-0477(1996)077<0437: TNYRP>2.0.CO; 2.

Li F, Wang H J. 2014. Autumn Eurasian snow depth, autumn Arctic sea ice cover and East Asian winter monsoon. Int J Climatol. 34:3616–3625

Li H, Wang H, Jiang D. 2017. Influence of October Eurasian snow on winter temperature over Northeast China. Adv Atmos Sci. doi:10.1007/s00376-016-5274-0

Li Q, Zhang R H, Wang Y. 2015. Interannual variation of the winter-time fog–haze days across central and eastern China and its relation with East Asian winter monsoon. Int. J. Climatol. 36 (1): 346–354, doi: 10.1002/joc.4350.

Robinson D.A., K F Dewey, R. Heim, Jr. 1993. Global snow cover monitoring: an update. Bulletin of the American Meteorological Society. 74: 1689-1696

Sun Bo. 2017. Seasonal evolution of the dominant modes of the Eurasian snowpack and atmospheric circulation from autumn to the subsequent spring and the associated surface heat budget . Atmos. Oceanic Sci. Lett., 10(3), 191-197, doi: 10.1080/16742834.2017.1286226.

Wang H. J., Chen H. P. 2016. Understanding the recent trend of haze pollution in eastern China: role of climate change. Atmos. Chem. Phys., 16: 4205–4211

Wang H. J., Chen H. P., Liu J. P. 2015. Arctic sea ice decline intensified haze pollution in eastern China. Atmos. Oceanic Sci. Lett., 8 (1): 1–9

Wang S. Y., Liu J. P., 2016. Delving into the relationship between autumn Arctic sea ice and central–eastern Eurasian winter

climate. Atmos. Oceanic Sci. Lett., 9(5), 366-374, doi: 10.1080/16742834.2016.1207482.

~~Xiao D., Li Y., Fan S. J., Zhang R. H., Sun J. R., Wang Y. 2015. Plausible influence of Atlantic Ocean SST anomalies on winter haze in China. Theor. Appl. Climatol. 122: 249–257~~

Xu X P, He S P, Li F, Wang H J. 2017. Impact of northern eurasian snow cover in autumn on the warm arctic–cold eurasia pattern during the following january and its linkage to stationary planetary waves. Climate Dynamics, 1-14. DOI 10.1007/s00382-017-3732-8

Xu X, Zhao T, Liu F, Gong S L, Kristovich D, Lu C, Guo Y, Cheng X, Wang Y, Ding G. 2016. Climate modulation of the Tibetan Plateau on haze in China. Atmospheric Chemistry and Physics. 16(3): 1365–1375

Yang Ting, Sun Yele, Zhang Wei, Wang Zifa, Wang Xiquan. 2016. Chemical characterization of submicron particles during typical air pollution episodes in spring over Beijing . Atmos. Oceanic Sci. Lett., 9(4), 255-262, doi: 10.1080/16742834.2016.1173509.

Yang Y., Liao H., Lou S. 2016. Increase in winter haze over eastern China in recent decades: Roles of variations in meteorological parameters and anthropogenic emissions. J. Geophys. Res. Atmos., 121: 13050–13065.

Yang Y., Russell L. M., Lou S., Liao H., Guo J., Liu Y., Singh B., Ghan S. J. 2017a. Dustwind interactions can intensify aerosol pollution over eastern China, Nat. Commun., 8, 15333, doi:10.1038/ncomms15333.

Yang Y., Wang H., Smith S. J., Ma P L, Rasch P J. 2017b. Source attribution of black carbon and its direct radiative forcing in China, Atmos. Chem. Phys., 17, 4319-4336, https://doi.org/10.5194/acp-17-4319-2017.

Yin Z. C., Wang H. J. 2016. The relationship between the subtropical Western Pacific SST and haze over North-Central North China Plain. International Journal of Climatology, 36: 3479–3491, DOI: 10.1002/joc.4570

Yin Z. C., Wang H. J., Chen H. P. 2017a. Understanding severe winter haze events in the North China Plain in 2014: roles of climate anomalies. Atmos. Chem. Phys., 17, 1641–1651, doi:10.5194/acp-17-1641-2017.

Yin Z C, Wang H J. 2017b. Role of Atmospheric Circulations on Haze Pollution in December 2016, Atmos. Chem. Phys., 17, 11673-11681, doi: 10.5194/acp-17-11673-2017

Yin Z. C., Wang H. J., Yuan D. M. 2015. Interdecadal increase of haze in winter over North China and the Huang-huai area

and the weakening of the East Asia winter monsoon. Chin. Sci. Bull. 60(15): 1395–1400 (in Chinese).

Yuan D M, Ma X H. 2017. The severe haze in 16—21 December 2016 and associated atmospheric circulation anomalies. Climatic and Environmental Research, accepted. (in Chinese)

Zhang F, Yan J R, Li J N, Wu K, Iwabuchi H, Shi Y N, 2017, A new radiative transfer method for solar radiation in a vertically internally inhomogeneous medium, Journal of Atmospherics Sciences,doi: http://journals.ametsoc.org/doi/abs/10.1175/JAS-D-17-0104.1

Zhang T Y, Chen H H, Sun Z B. 2007. The Relationship between Autumn- time Eurasian Snow Cover and Winter-time NH Circulation. Acta Geographica Sinica, 62(7): 728-741.

Zhou Wen. 2017. Impact of Arctic amplification on East Asian winter climate,Atmospheric and Oceanic Science Letters, 10:5, 385-388, DOI: 10.1080/16742834.2017.1350093

Zou Y F, Wang Y H, Zhang Y Z, and Koo J H. 2017. Arctic sea ice, Eurasia snow, and extreme winter haze in China. Science Advances, 3 (3): e1602751, DOI: 10.1126/sciadv.1602751

Figures and Tables caption

Table 1 The CC between the DHD_{CNC} and SoilM index in October-November (ON) and December (Dec). OS means 'original sequence', and 'DT' means that the linear trend was removed. '*' indicates the result passed the 95% confidence level, and '**' indicates the CC passed the 99% confidence level.

Table 2 The CC between the DHD_{CNC} and I_{LS1} (I_{LS2}). OS means 'original sequence', and 'DT' means that the linear trend was removed. '*' indicates the result passed the 95% confidence level, and '**' indicates the CC passed the 99% confidence level.

Figure 1 (a) the variation of the normalized DHD_{CNC} (black) and SC_{ES} (blue) from 1979 to 2016 after detrending and the 21-yr running correlation coefficient (CC) between the DHD_{NH} and SC_{ES} before (solid, red) and after (dash, red) detrending. (b) The CC between the DHD_{CNC} and snow cover from 1979 to 2016 after detrending. The black dots indicate CCs

exceeding the 95% confidence level (t test). The black box represents the ES area. The subscript "dt" and "OS" in panel (a) represented the CC was calculated by the detrending and original sequence.

Figure 2 The CC between the SC_{ES} and snow cover (a) from 1979 to 1997 and (b) from 1998 to 2016. The black dots indicate the CC exceeded the 95% confidence level (t test). The black box represents the ES area. The linear trend is removed. The green lines indicate that the interannual variations in snow cover were obvious in this region.

Figure 3 The CC between the SC_{ES} and Z200 (shading) and U200 (contour) in December from 1998 to 2016. The black dots indicate the CC exceeded the 95% confidence level (t test). The green box represents the ES area. The linear trend is removed.

Figure 4 The CC between the SC_{ES} and Z500 (shading, exceeding 90%, 95% and 99% confidence level), stream function (contour), and wave activity flux (arrow) in December from 1998 to 2016. The green box represents the ES area. The linear trend is removed.

Figure 5 The CC between the SC_{ES} and (a) BLH (shading), surface omega (contour), (b) wind at 850 hPa (arrow), surface wind speed (shading), and surface relative humidity (contour), and (c) SLP (contour) and SAT (shading) in December from 1998 to 2016. The black dots indicate the CC exceeded the 95% confidence level (t test). The linear trend is removed.

Figure 6 The CC between the SC_{ES} and Z200 (shading) and U200 (contour) in December from 1979 to 1997. The black dots indicate the CC exceeded the 95% confidence level (t test). The green box represents the ES area. The linear trend is removed.

Figure 7 The CC between the SC_{ES1} and Z500 (shading, exceeding 90%, 95% and 99% confidence level), stream function (contour), and wave activity flux (arrow) in December from 1979 to 1997. The green box represents the ES area. The linear trend is removed.

Figure 8 The CC between the SC_{ES1} and (a) BLH (shading) and surface omega (contour), (b) wind at 850 hPa (arrow), surface wind speed (shading), and surface relative humidity (contour), and (c) SLP (contour) and SAT (shading) in December from 1979 to 1997. The black dots indicate the CC exceeded the 95% confidence level (t test). The linear trend is removed.

Figure 9 The CC between the SC_{ES} and soil moisture in (a) October-November and (c) December from 1979 to 1997, and in

(b) October-November and (d) December from 1998 to 2016. The black dots indicate the CC exceeded the 95% confidence level (t test). The linear trend is removed. The green boxes (RM1 and RM2) are the significantly correlated areas, which were used to calculate the SoilM index.

Figure 10 The CC between the SoilM index and Z500 (shading, exceeding 90%, 95% and 99% confidence level), stream function (contour), and wave activity flux (arrow) in (a) October-November and (c) December from 1979 to 1997 and in (b) October-November and (d) December from 1998 to 2016. The green box represents the ES area. The linear trend is removed.

Figure 11 The CC between the SC_{ES} and (a) longwave radiation and (c) shortwave radiation in October-November from 1979 to 1997 and the CC between the SC_{ES} and (b) longwave radiation and (c) shortwave radiation in October-November from 1998 to 2016. The black dots indicate the CC exceeded the 95% confidence level (t test). The linear trend is removed. The green boxes (RL and RS) are the significantly correlated areas, which were used to calculate the I_{LS1} (I_{LS2}).

Figure 12 The CC between the SC_{ES} and SAT (shading) and SLP (contour) in October-November (a) from 1979 to 1997 and (b) from 1998 to 2016. The black dots indicate the CC exceeded the 95% confidence level (t test). The green box represents the ES area. The linear trend is removed.

Figure 13 The CC between (a) I_{LS1}, (b) I_{LS2} and Z500 (shading) and U200 (contour) in December. The black dots indicate the CC exceeded the 95% confidence level (t test). The linear trend is removed.

Figure S1. The CC between the SC_{ES} and the September (a), October (b) and November (c) Arctic sea ice from 1979 to 1997 after detrending. The black dots indicate the CC exceeded the 95% confidence level (t test).

Figure S2. The CC between the SC_{ES} and the September (a), October (b) and November (c) Arctic sea ice from 1998 to 2016 after detrending. The black dots indicate the CC exceeded the 95% confidence level (t test).

Figure S3. Diagram of the associated physical mechanisms. Near surface, the ON radiation (contour) and soil moisture (shade) were influenced by the SCES. On the mid-high level, the teleconnected Rossy wave-like pattern propagated into the Central North China, representing by Z500 (shade), stream function (contour) and wave activity flux (arrow). Finally, the local anti-cyclonic circulation near surface (arrow) led to weak ventilation conditions in December.

405

410

415

Table 1 The CC between the DHD_{CNC} and SoilM index in October-November (ON) and December (Dec). OS means 'original sequence', and 'DT' means that the linear trend was removed. '*' indicates the result passed the 95% confidence level, and '**' indicates the CC passed the 99% confidence level.

CC	1979–1997		1998–2016	
	OS	DT	OS	DT
ON	0.15	0.14	0.77**	0.69**
Dec	0.13	–0.10	0.78**	0.69**

420

425

Table 2 The CC between the DHD_{CNC} and I_{LS1} (I_{LS2}). OS means 'original sequence', and 'DT' means that the linear trend was removed. '*' indicates the result passed the 95% confidence level, and '**' indicates the CC passed the 99% confidence level.

CC	1979–1997		1998–2016	
	OS	DT	OS	DT
I_{LS1}	–0.67**	0.07		
I_{LS2}			–0.78**	–0.72**

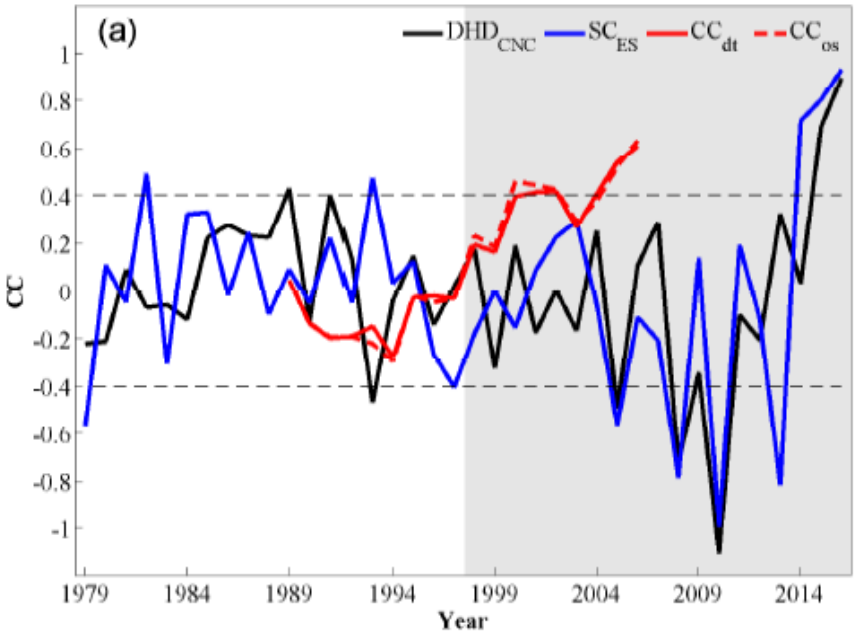

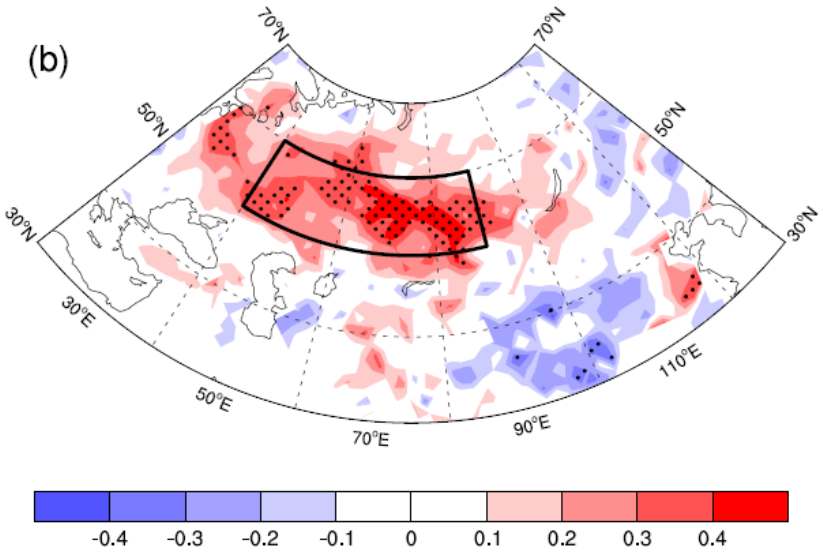

Figure 1 (a) the variation of the normalized DHD_{CNC} (black) and SC_{ES} (blue) from 1979 to 2016 after detrending and the 21-yr running correlation coefficient (CC) between the DHD_{NH} and SC_{ES} before (solid, red) and after (dash, red) detrending. (b) The CC between the DHD_{CNC} and snow cover from 1979 to 2016 after detrending. The black dots indicate CCs exceeding the 95% confidence level (t test). The black box represents the ES area. The subscript "dt" and "OS" in panel (a) represented the CC was calculated by the detrending and original sequence.

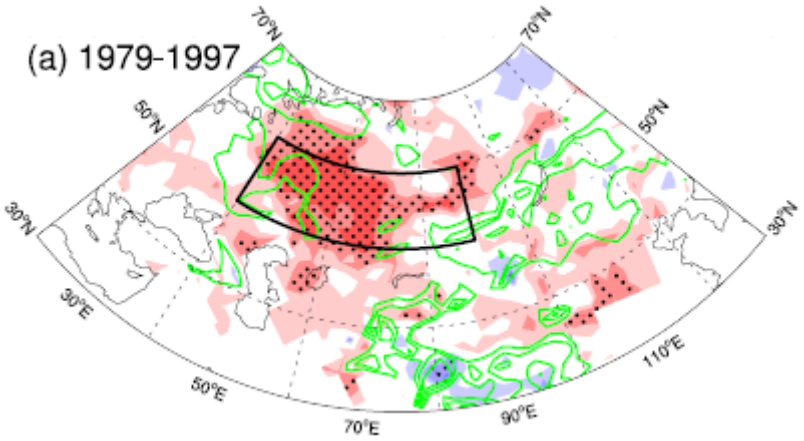

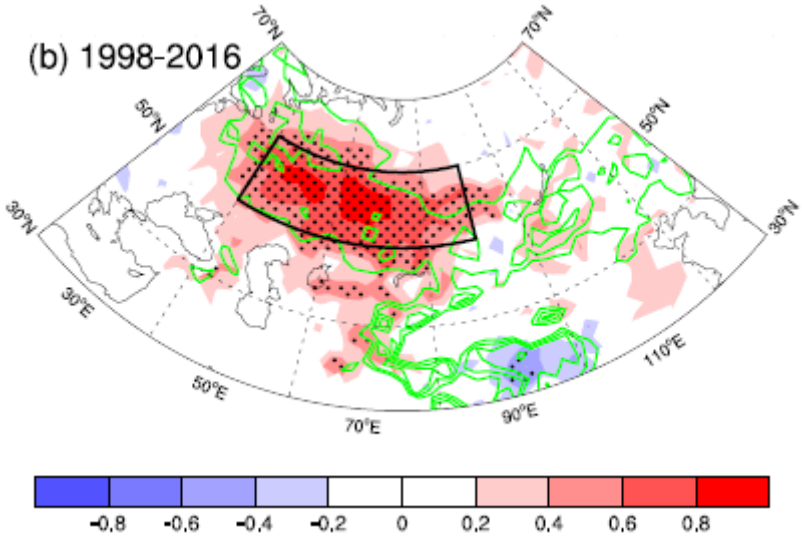

Figure 2 The CC between the SC_{ES} and snow cover (a) from 1979 to 1997 and (b) from 1998 to 2016. The black dots indicate the CC exceeded the 95% confidence level (t test). The black box represents the ES area. The linear trend is removed. The green lines indicate that the interannual variations in snow cover were obvious in this region.

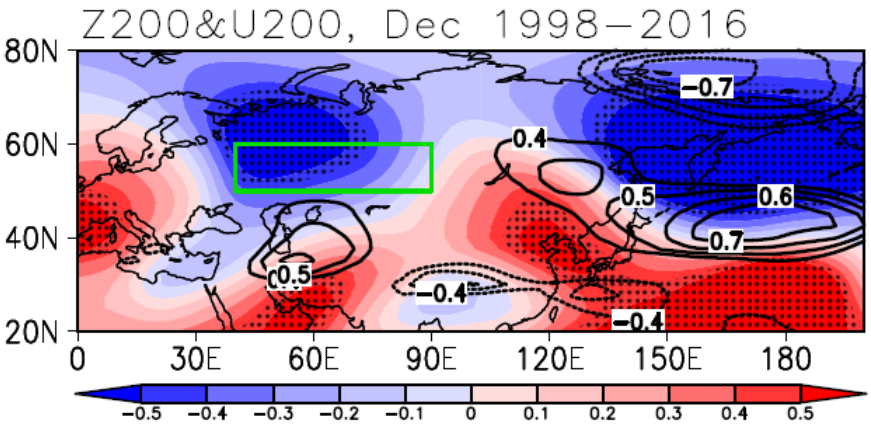

Figure 3 The CC between the SC_{ES} and Z200 (shading) and U200 (contour) in December from 1998 to 2016. The black dots indicate the CC exceeded the 95% confidence level (t test). The green box represents the ES area. The linear trend is removed.

480

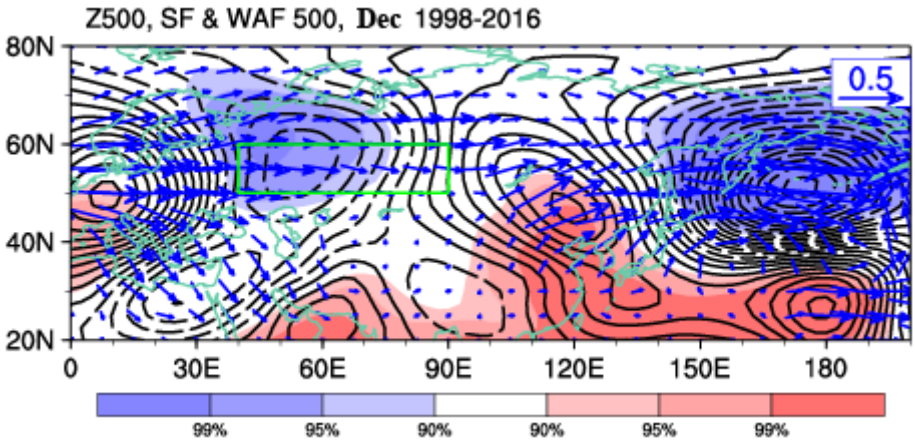

Figure 4 The CC between the SC_{ES} and Z500 (shading, exceeding 90%, 95% and 99% confidence level), stream function (contour), and wave activity flux (arrow) in December from 1998 to 2016. The green box represents the ES area. The linear trend is removed.

485

490

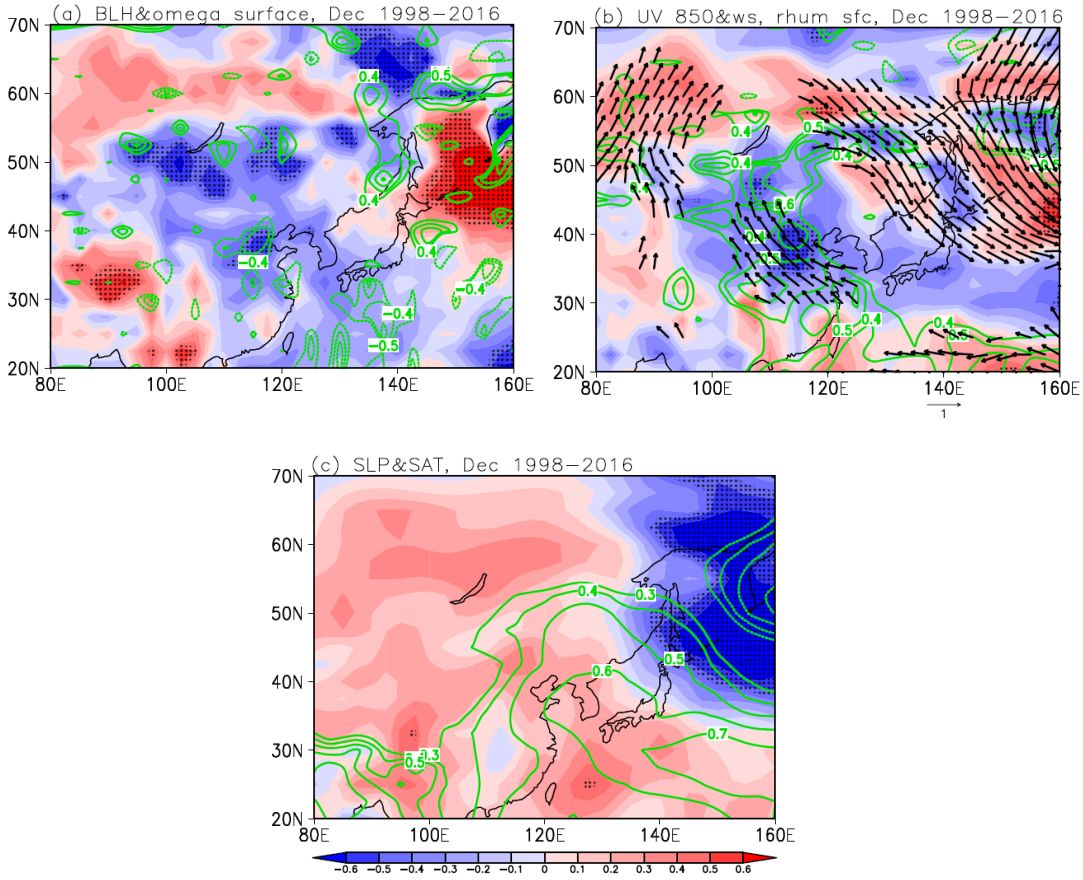

Figure 5 The CC between the SC_{ES} and (a) BLH (shading), surface omega (contour), (b) wind at 850 hPa (arrow), surface wind speed (shading), and surface relative humidity (contour), and (c) SLP (contour) and SAT (shading) in December from 1998 to 2016. The black dots indicate the CC exceeded the 95% confidence level (t test). The linear trend is removed.

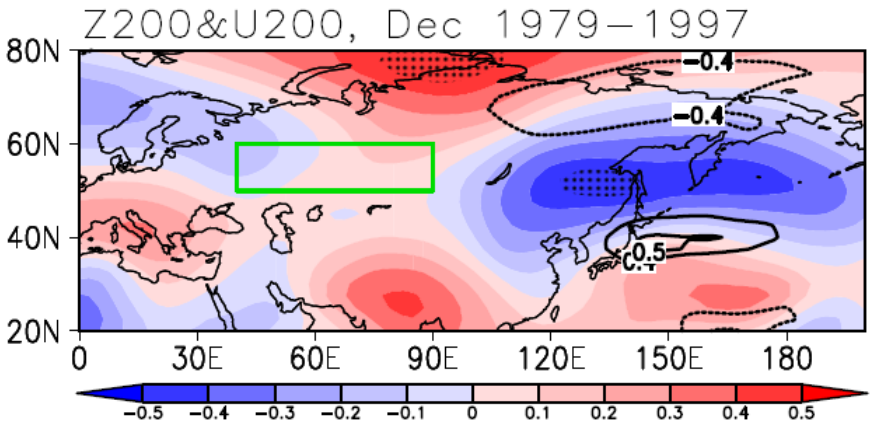

Figure 6 The CC between the SC_{ES} and Z200 (shading) and U200 (contour) in December from 1979 to 1997. The black dots indicate the CC exceeded the 95% confidence level (t test). The green box represents the ES area. The linear trend is removed.

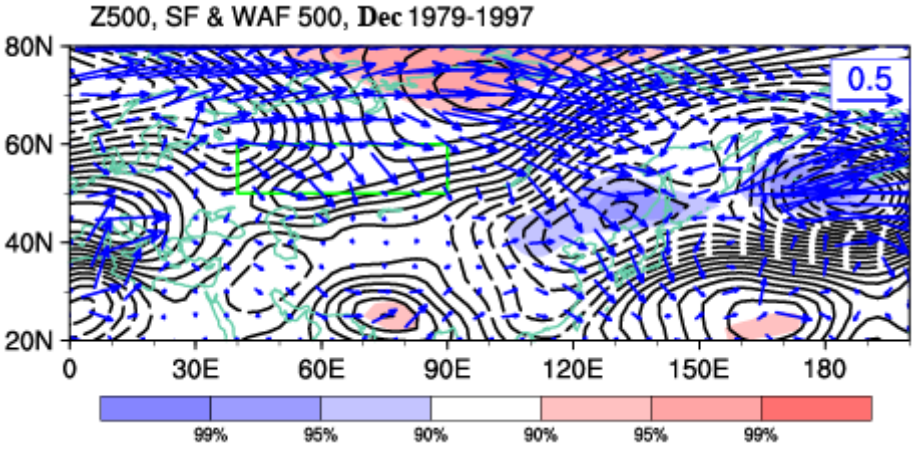

Figure 7 The CC between the SC_{ES+} and Z500 (shading, exceeding 90%, 95% and 99% confidence level), stream function (contour), and wave activity flux (arrow) in December from 1979 to 1997. The green box represents the ES area. The linear trend is removed.

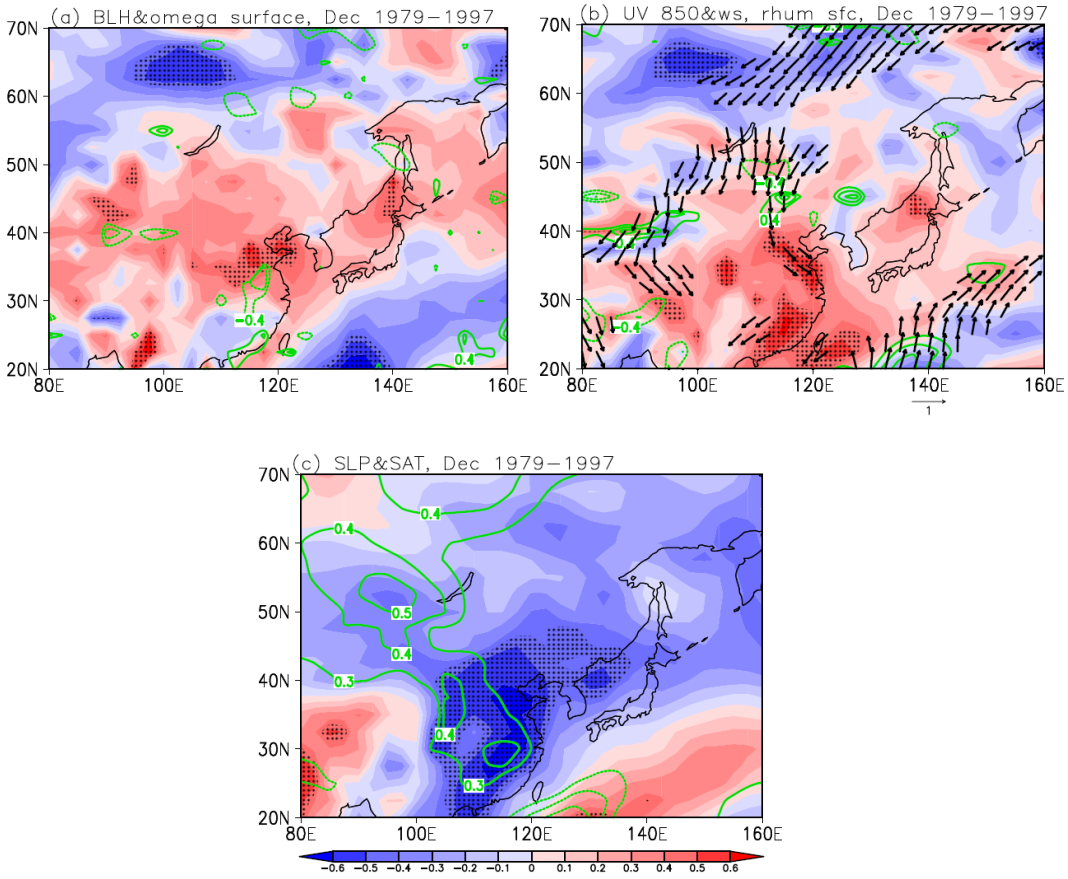

Figure 8 The CC between the SC_{ES+} and (a) BLH (shading) and surface omega (contour), (b) wind at 850 hPa (arrow), surface wind speed (shading), and surface relative humidity (contour), and (c) SLP (contour) and SAT (shading) in December from 1979 to 1997. The black dots indicate the CC exceeded the 95% confidence level (t test). The linear trend is removed.

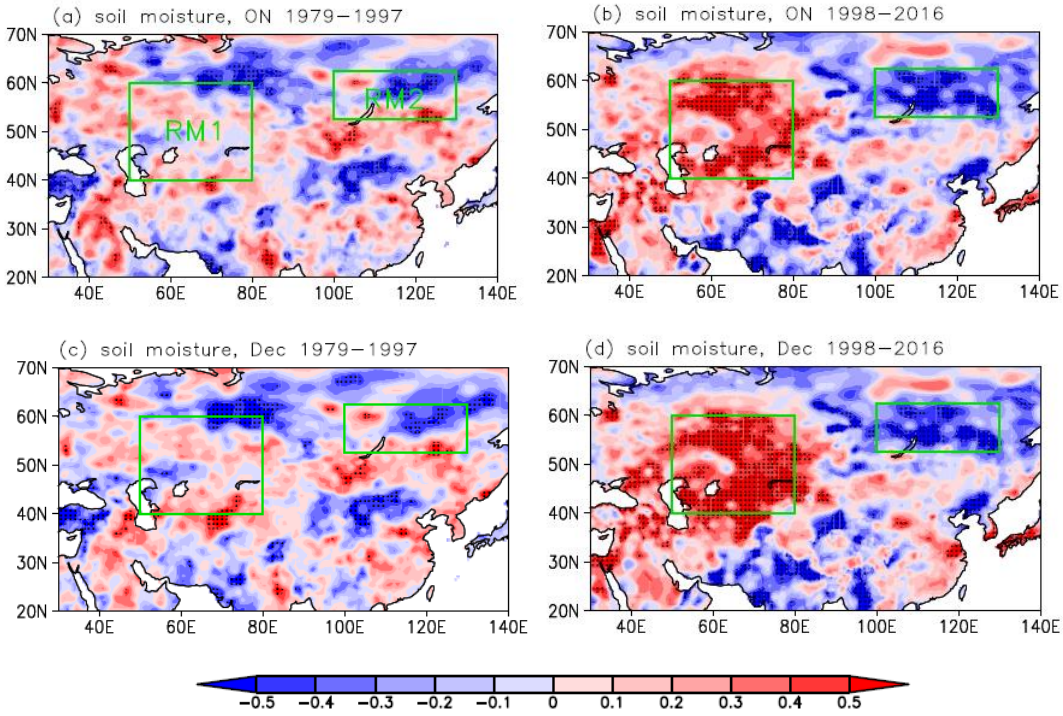

Figure 9 The CC between the SC_{ES} and soil moisture in (a) October-November and (c) December from 1979 to 1997, and in (b) October-November and (d) December from 1998 to 2016. The black dots indicate the CC exceeded the 95% confidence level (t test). The linear trend is removed. The green boxes (RM1 and RM2) are the significantly correlated areas, which were used to calculate the SoilM index.

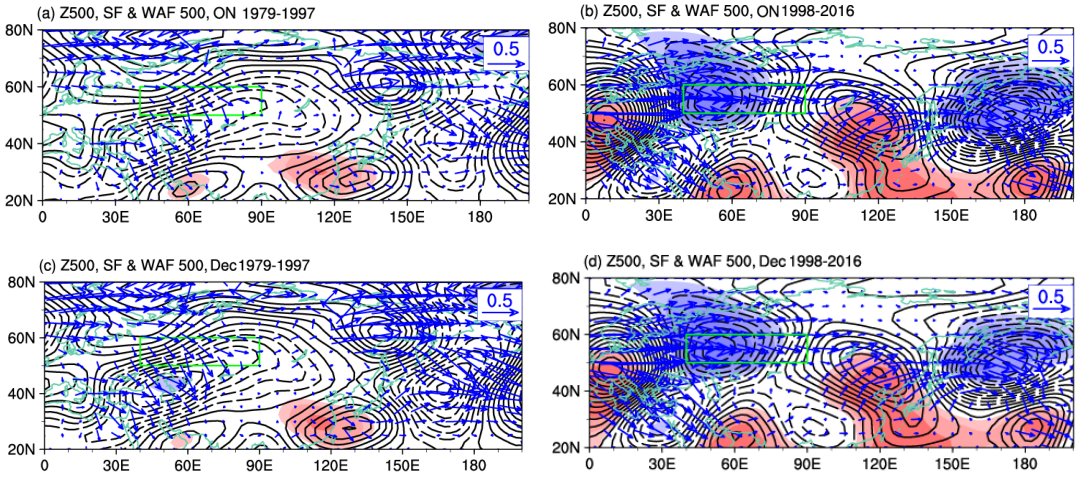

Figure 10 The CC between the SoilM index and Z500 (shading, exceeding 90%, 95% and 99% confidence level), stream function (contour), and wave activity flux (arrow) in (a) October-November and (c) December from 1979 to 1997 and in (b) October-November and (d) December from 1998 to 2016. The green box represents the ES area. The linear trend is removed.

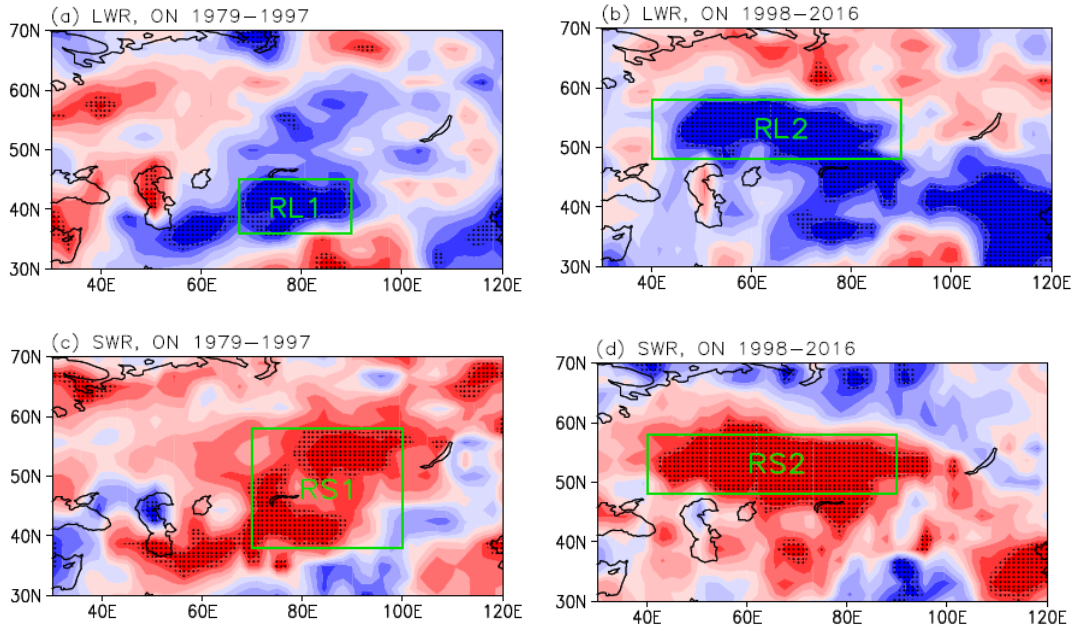

Figure 11 The CC between the SC_{ES} and (a) longwave radiation and (c) shortwave radiation in October-November from 1979 to 1997 and the CC between the SC_{ES} and (b) longwave radiation and (c) shortwave radiation in October-November from 1998 to 2016. The black dots indicate the CC exceeded the 95% confidence level (t test). The linear trend is removed. The green boxes (RL and RS) are the significantly correlated areas, which were used to calculate the I_{LS1} (I_{LS2}).

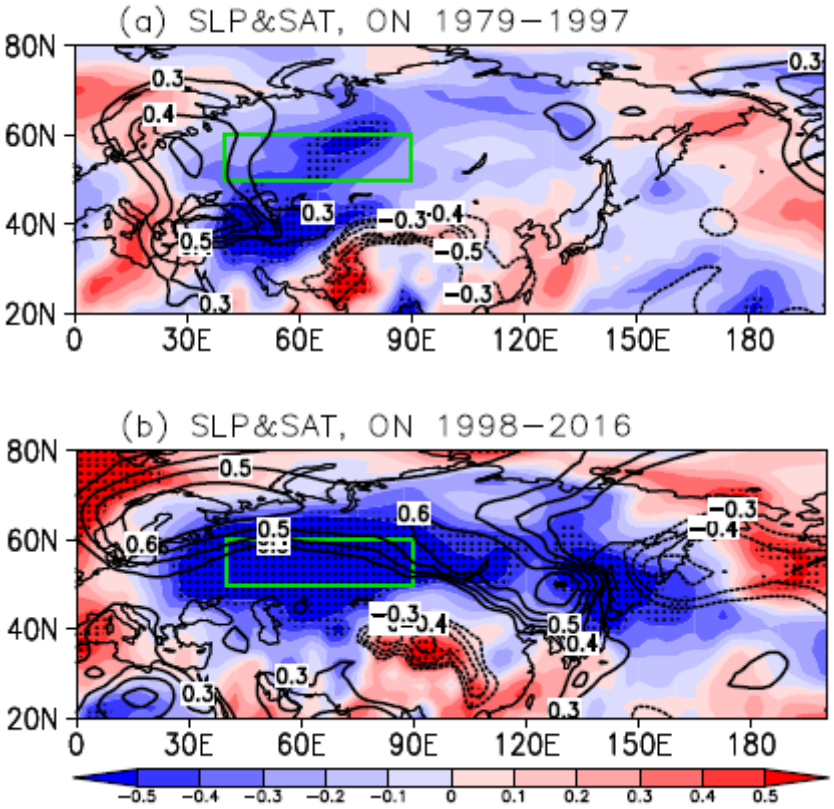

Figure 12 The CC between the SC_{ES} and SAT (shading) and SLP (contour) in October-November (a) from 1979 to 1997 and (b) from 1998 to 2016. The black dots indicate the CC exceeded the 95% confidence level (t test). The green box represents the ES area. The linear trend is removed.

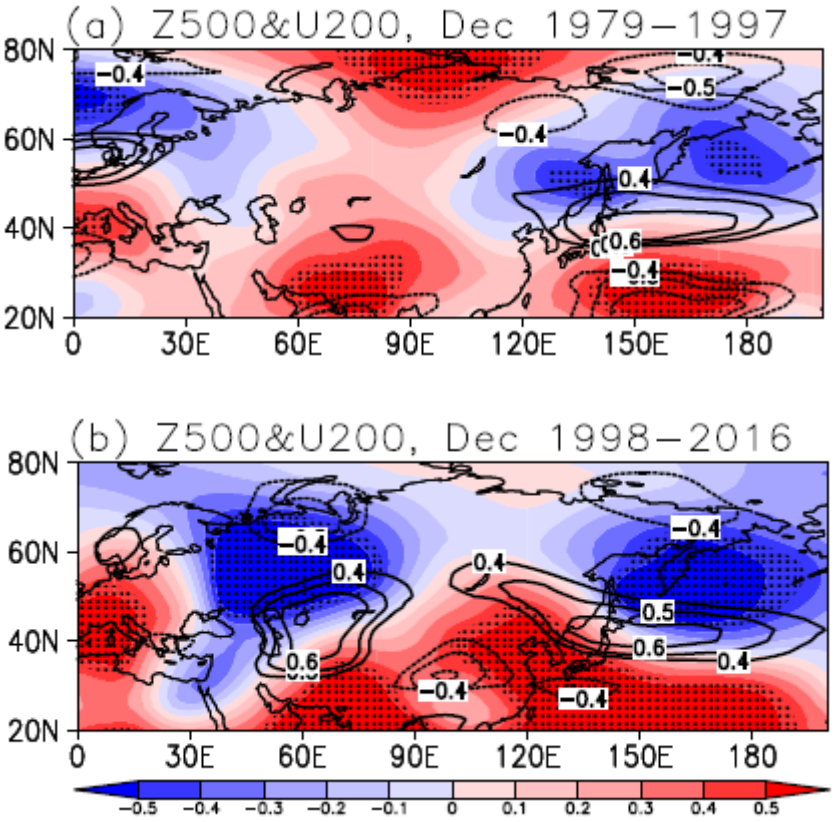

Figure 13 The CC between (a) I_{LS1}, (b) I_{LS2} and Z500 (shading) and U200 (contour) in December. The black dots indicate the CC exceeded the 95% confidence level (t test). The linear trend is removed.